Comparison of different silica sources in the development of plasma sprayed 45S5 bioactive glass coatings

E. Cañas[a,*], M. Díaz[b], C. Alcázar[b], M.J. Orts[a], R. Moreno[b], E. Sánchez[a]

[a]Instituto de Tecnología Cerámica (ITC), Universitat Jaume I (UJI), 12006, Castellón, Spain

[b]Instituto de Cerámica y Vidrio (ICV), Consejo Superior de Investigaciones Científicas (CSIC), Universidad Autónoma de Madrid, 28049, Madrid, Spain

Eugeni Cañas Recacha
Email: eugeni.canas@itc.uji.es
Telephone number: (+34) 964342424
Fax number: (+34) 964342425
(* corresponding author)

María Díaz Fernandez
Email: mariadifer@icv.csic.es

Carmen Alcázar Rodrigo
Email: carmen.alcazar@icv.csic.es

María José Orts Tarí
Email: mariajose.orts@itc.uji.es

Rodrigo Moreno Botella
Email: rmoreno@icv.csic.es

Enrique Sánchez Vilches
Email: enrique.sanchez@itc.uji.es

Abstract

45S5 bioactive glass coatings were deposited by plasma spraying from liquid feedstocks. In these feedstocks, the SiO_2 needed to achieve the 45S5 bioactive glass composition has been provided either as tetraethyl orthosilicate (typical precursor of glasses by sol–gel), or as colloidal silica suspension or mixtures of both sources. The synthesised materials were analysed in terms of rheology and sedimentation tests, and subsequently deposited onto metallic substrates under two different spraying distances. The resulting coatings were characterised on the basis of microstructure and phase nature.

All feedstocks developed preserved the composition of the 45S5 bioactive glass and showed adequate viscosity and stability to be transported and injected into the plasma plume. However, different coating microstructures were achieved when using tetraethyl orthosilicate or colloidal silica suspensions. Besides, regardless the source of silica an improvement of the coatings microstructure and phase nature have also been observed when the spraying distance was significantly reduced.

Keywords: 45S5 bioactive glass; Plasma spraying; Silica; Glass suspension; Glass solution; Coating microstructure

1. Introduction

The 45S5 bioactive glass or Bioglass®, discovered by Prof. Hench, was the first bioactive material capable of developing new bone tissue when in contact with it [1]. 45S5 glass is basically a soda–lime glass including some phosphorous with the following composition 45% SiO_2, 24.5% CaO, 24.5% Na_2O and 6% P_2O_5, in wt% [2,3]. Nevertheless, from the discovery of this glass until now, a lot of research has been performed proposing modified compositions of this material depending on the synthesis method or the final application [4–9]. Consequently, nowadays there is a growing family of bioactive glasses based on mixtures of glass former and modifier oxides such as SiO_2–CaO–MgO–Na_2O–K_2O–ZnO–B_2O_5–P_2O_5.

Among all the emerging applications of these materials in the field of medicine, one of them is the utilisation of bioactive glasses as a prosthesis coating being plasma spraying the most common method employed for that purpose [1,10,11]. Up to now, the study and deposition of plasma sprayed bioactive glass coatings were done using powder and suspension feedstocks through Atmospheric Plasma Spraying (APS) and Suspension Plasma Spraying (SPS) processes respectively. These glass powder feedstocks were usually obtained either by the melting and quenching method or by sol–gel [12,13], and then directly used in the form of powder or suspended in an organic medium when their particle size is lower than 10 μm in order to preserve some stability. Typical organic media employed are ethanol or glycols [14–16], since bioactive glasses tend to react with water (leaching) leading to a cation exchange and consequently modifying their final composition [17].

Nevertheless, precursor solutions have started to be used as a feedstock in the field of plasma spraying, method referred as Solution Precursor Plasma Spraying (SPPS) [18,19].

The utilisation of this method allows an easier exploration of different material compositions as well as the deposition of advanced coatings (thinner and nanostructured) with a homogeneous and dense microstructure [20,21]. These aspects can provide significant advantages to obtain suitable coatings from bioactive glasses. In addition, SPPS permits to work with purer feedstocks since further powder or suspension elaboration steps which can introduce impurities or contaminants, such as milling, are removed and also allows the use of water as a solvent, since there is no problem of leaching from the precursors unlike the bioactive glass powders, resulting in feedstocks which are safer and easier to handle. SPPS has been used to deposit coatings from a wide variety of materials for different applications such as thermal barrier coatings [22–24], solid fuel cells [25,26], photocatalytic coatings [27,28] or biocoatings [29–33].

During the last years, authors of the present work also started to address the deposition of 45S5 bioactive glass coatings from liquid feedstocks (suspension and solution of precursors) [16,33]. Despite the presence of crystalline phases, promising results were obtained when using SPPS, since the coating displayed good microstructure with higher adhesion [33]. Moreover, the SPPS bioactive glass coating showed a positive reaction when immersed in Simulated Body Fluid (SBF) [33].

As mentioned in the literature, the processes related to the material formation and deposition that take place inside the plasma plume once the solution feedstock is injected are complex (droplets evaporation and break up, gelation, precipitation, pyrolysis, sintering, melting, crystallisation) and not well–understood [22–24,34]. Therefore, the aim of the present work is to simplify the deposition mechanisms that take place in the plasma plume based on a new feedstock approach in which tetraethyl orthosilicate (TEOS), a metallic alkoxide usually employed as a precursor of SiO_2, was partially or

even totally replaced by colloidal silica suspensions. In that way, after feedstock injection into the plasma plume, only the liquid media must evaporate and then the colloidal silica particles can melt, react with the other diluted alkoxide and salts and act as a nucleus of glass formation. The developed feedstock materials were characterised in terms of viscosity and stability and deposited by plasma spraying. Then, all coatings were analysed by scanning electron microscopy and X–ray diffraction with the aim of assessing the possible effect of TEOS replacement on coatings microstructure. For the sake of comparison, the bioactive glass solution from previous work [33], without colloidal silica, was also prepared, characterised and sprayed.

2. Experimental

2.1. Feedstocks preparation

45S5 bioactive glass was used as target composition of feedstocks. Starting from previous work [33], an aqueous–based solution was prepared employing tetraethyl orthosilicate (TEOS) ($C_8H_{20}O_4Si$ synthesis grade, Merck, Germany), triethyl phosphate (TEP) ($C_6H_{15}O_4P$ synthesis grade, Merck, Germany), calcium nitrate ($Ca(NO_3)_2 \cdot 4H_2O$ >99%, VWR Chemicals, USA) and sodium nitrate ($NaNO_3$ >99%, Sigma–Aldrich, USA) as precursors of SiO_2, P_2O_5, CaO and Na_2O respectively. First, nitric acid (Tritripur, Merck, Germany) was mixed with water resulting in an acidic solution with a concentration of 0.2 M to hydrolyse TEOS and TEP. Then, TEOS was added drop by drop to the acidic solution under magnetic stirring at 500 rpm and, after the addition of the whole reagent, the mixture was kept in agitation for half an hour until its total clarification. Next, TEP was added in the same way as TEOS (drop by drop, stirring at 500 rpm and a mixture time of 30 minutes). Finally, both salts were gradually added to the solution. The

procedure was the same for the two salts and involved the addition of the reagent to the solution under magnetic stirring at 700 rpm and after that, the resulting mixture was kept under agitation for 1 hour to ensure complete dissolution of the reagent. Following this procedure, first calcium nitrate was added and then sodium nitrate. To achieve the 45S5 glass composition, the amount of TEOS was determined based on a molar ratio water to TEOS of 18, and for the rest of reagents, their amounts were determined from the glass composition by stoichiometry. The resulting solution (referred as GS), with a total concentration of precursor of 4M, was kept inside a sealed glass container at a temperature of 5 ºC [35].

After the synthesis of GS, different liquid feedstocks were prepared by replacing partially (50 %) or totally (100 %) TEOS by colloidal silica suspensions. For the replacement, two commercial suspensions were used, which are described below.

- Levasil CT17 PDL (AkzoNobel, USA), colloidal silica aqueous–based suspension, with a solids content of 30 wt% and stabilised at a pH of ≈3.
- Ludox TM–40 (Sigma–Aldrich, USA), colloidal silica aqueous–based suspension, with a solids content of 40 wt% and stabilised at a pH of ≈9.

The procedure followed for feedstocks preparation was the same as for the GS with the difference that in all cases the colloidal silica suspensions were added at the final step of the procedure and not at the beginning as TEOS. Moreover, these feedstocks were also kept at low temperature (5 ºC) inside a sealed glass container. Table 1 shows the references for the new feedstocks prepared.

Table 1. References of the new developed feedstocks

Feedstock reference	LE05	LU05	LE1	LU1
Silica suspension	Levasil CT17	Ludox–TM40	Levasil CT17	Ludox–TM40
Degree of substitution	50%	50%	100%	100%
Feedstock pH	1.15	1.35	1.14	1.33

2.2. Characterisation of the developed feedstocks

The chemical composition of the developed materials was determined. For that purpose, a sample of each feedstock was dried in a stove at 100 ºC and the resulting powder was sintered at 700 ºC. After sintering, each sample was dry milled and fused into bead; and their chemical composition was assessed by wavelength dispersive X–ray fluorescence spectrometry (XRF) (AXIOS, PANalytical, The Netherlands) with a Rh anode tube and certified reference materials.

When spraying liquid feedstocks, two different requirements must be fulfilled [36]:

- The feedstock must have low viscosity to make it possible its transport through the pipes and its injection into the plasma jet.
- The feedstock must have good physical and chemical stability to preserve the properties and characteristics of the material and hence to avoid the modification of coating properties with time.

For that reason, the stability of all feedstocks was assessed through a rheological study. This study, performed at 298 K by using a double–cone and plate system, was done in a rheometer (Haake RS50, Thermo Scientific, Germany) which controlled the shear rate

(CR) from 0 to 1000 s^{-1} in 5 min, maintaining it at 1000 s^{-1} for 1 min and downloading it from 1000 to 0 s^{-1} in 5 min. Since colloidal silica suspensions were introduced in the feedstocks, two new tests were carried out in order to complete the assessment of feedstocks stability. On the one hand, the variation of the zeta potential with pH was determined for these commercial suspensions. For that purpose, aliquots of each suspension were first diluted in potassium chloride (KCl) 0.01 M and then the pH of each diluted aliquot was adjusted with hydrochloric acid (HCl) and potassium hydroxide (KOH). Finally, the zeta potential for each pH value was determined in a dynamic light scattering (Zetasizer NanoZS, Malvern, Great Britain). On the other hand, sedimentation tests were performed to those feedstocks containing the colloidal silica after its preparation. The tests were carried out in a multiple light scattering equipment (TurbiScan Classic MA2000, Formulaction, France), taking data during one hour of measurement.

2.3. Deposition and characterisation of coatings

Once the liquid feedstocks were prepared and characterised, the next step was their deposition by plasma spraying. The facility used to deposit the coatings comprised a single cathode plasma torch (F4–MB, Sulzer Metco, Switzerland) which is coupled to a six–axis robot (IRB 1400, ABB, Switzerland) for movement control. With the aim of injecting the liquid feedstocks, a home–made injection system is also attached to the plasma gun. This system is composed of two pressurised containers, which force the liquid to flow through an injector due to a pressure difference, injecting the liquid feedstock in a radial way to the plasma jet. A filter was placed into the injector to remove large agglomerates and possible contaminations that can clog the injector. Details about this facility can be found in published works [37,38].

In order to deposit the coatings, AISI type 304 stainless steel substrates disk shaped with a diameter of 25 mm were used. The substrate preparation comprised a sand–blasting first step with black corundum at a pressure of 4.2 bar and a second step of cleaning with ethanol in an ultrasonic bath. After that, roughness of the substrates was measured with a roughness tester (HOMMELWERKE T8000, Hommelwerke GmbH, Germany) being the obtained roughness (R_a) 2.2 ± 0.1 μm.

Concerning the spraying of the feedstocks, the parameters used are shown in table 2. Basically, these parameters are the same as described in previous research [33]. The only difference deals with the spraying distances employed. As shown in the previous research, the spraying distance has a great effect on the resulting microstructure of the coatings, giving rise to better coatings for a lower distance (higher adhesion to the substrate). Therefore, in the present work, the smallest distance was maintained (70 mm) and a shorter one (40 mm) was tested in order to study different microstructures and check if an improvement of the coatings' microstructure took place.

Furthermore, before feedstocks deposition, a bond coat of TiO_2 powder was deposited by atmospheric plasma spraying (APS) from commercial anatase powder (Metco 102, Oerlikon Metco, Switzerland), with particle size distribution between 10–55 μm to enhance the glass top coating adhesion [39,40]. The spraying conditions used were given by the supplier and are also shown in table 2. As it can be seen, the spraying distance is longer than that used for the liquid feedstocks, in order to completely melt the powder particles. Moreover, the bond coated substrates were preheated between 300 °C and 350 °C in order to further improve adhesion [41].

Table 2. Plasma spray conditions used for the deposition of the TiO_2 powder bond coat and each glass feedstock

Parameter	TiO_2 bond coat (Powder)	45S5 glass liquid feedstocks
Ar (slpm*)	38	25
H_2 (slpm*)	14	15
Intensity (A)	600	600
Spraying distance (mm)	120	40–70
Scan velocity (mm s^{-1})	1000	1250
Number of torch scans	2	5
Nozzle diameter (mm)	1.80	–
Powder flow rate (g s^{-1})	0.75	–
Injector diameter (μm)	–	150
Suspension flow rate (ml s^{-1})	–	0.55

* *Standard litre per minute*

Finally, the coatings deposited from the different liquid feedstocks were examined and compared by field emission gun environmental scanning electron microscope (FEG–ESEM) (QUANTA 200FEG, FEI Company, USA). First, surface micrographs were taken and then the coatings were cut and metallographically prepared to observe their cross–section. For the latter, each coating was carefully cut with a diamond–coated and water–cooled disk (M4D18, Struers, Denmark) in an automatic cutting machine (Secotom–10, Struers, Denmark) and mounted with epoxy resin (Kit Epofix, Struers, Denmark) [42,43]. Then, the mounted samples were polished with a polishing machine (TegraPol–35,

Struers, Denmark) using different clothes with their corresponding abrasive slurry (Struers, Denmark) and different times as shown below in table 3.

Table 3. Consumables used for the polishing step, supplied by Struers

Clothes	Abrasive slurry	Grit size	Application time
MD–Piano 220	Resin bonded diamond*	68 μm	60 s
MD–Allegro	Diamond	15–6 μm	300 s
MD–Dur	Diamond	9–1 μm	330 s
MD–Mol	Diamond	< 3 μm	330 s
MD–Nap	Diamond	< 1 μm	360 s

**Abrasive incorporated in the cloth. Water–cooled*

At the end, the samples were cleaned in an ultrasonic bath with distilled water and dried in an oven at 80 ºC for 2 hours.

Furthermore, the distribution of elements of the bioactive glass composition (Si, Ca, Na and P) was studied by means of energy–dispersive X–ray microanalysis (EDS) coupled to an electronic microscope (Quattro S, ThermoFisher Scientific, The USA). The polished cross–section samples used to obtain the micrographs were carbon coated by sputtering, placed inside the microscope and an X–ray mapping of elements was done under high vacuum conditions.

Finally, the amorphous/crystalline nature of the obtained coatings was assessed by X–ray diffraction (XRD) using a diffractometer (Advance diffractometer, Bruker Theta–Theta, Germany) with Cu Kα radiation and performing the measurement over a range of 2θ between 10° and 80°.

3. Results and discussion

3.1. Feedstocks composition and stability

The composition of the feedstocks resulting from their chemical analyses is shown in table 4 together with the composition of the nominal 45S5 bioactive glass.

Table 4. Solution feedstocks composition

Composition (wt%)	**SiO_2**	**CaO**	**Na_2O**	**P_2O_5**
45S5 glass	45.0	24.5	24.5	6.0
Glass solution [33]	46.0	23.3	25.5	5.3
Levasil substitution*	49.6	21.6	24.1	4.8
Ludox substitution*	44.5	23.7	26.4	5.5

*Average between the composition of feedstocks with partial and total replacement

As explained in previous work [33], the composition of the bioactive glass solution was very close to that of the nominal glass. In addition, using both colloidal silica suspensions (Levasil CT17 and Ludox TM–40), indistinctly of the degree of substitution the composition of the resulting new feedstocks remains very similar to the reference composition.

The next step was the assessment of feedstocks stability. In first place the colloidal stability of silica suspensions as a function of pH was studied through zeta potential measurements. Figure 1 shows the evolution of zeta potential with pH for both colloidal suspensions (Levasil CT17 PDL in figure 1a and Ludox TM–40 in figure 1b).

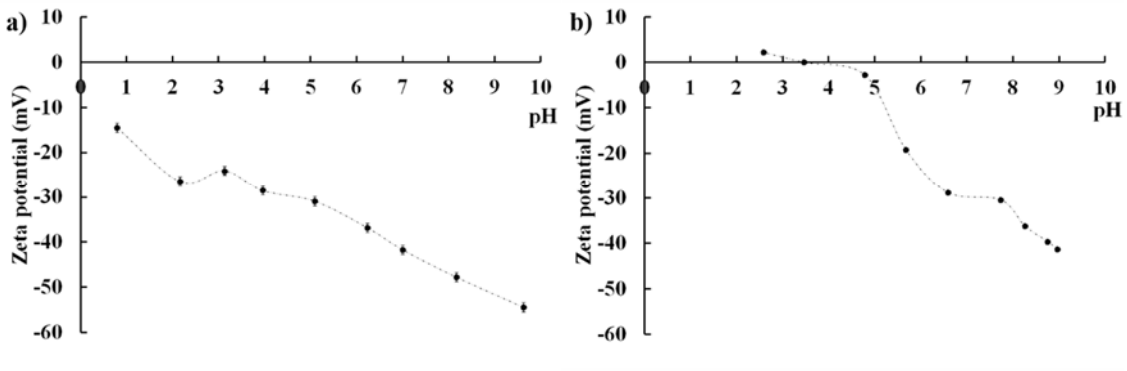

Figure 1. Zeta potential of colloidal silica suspensions as a function of pH. a) Levasil CT17 PDL and b) Ludox TM–40

For both suspensions, it can be seen that the more basic the medium the higher the particle charge (in absolute value) and thus, the higher the repulsion between particles. In the case of the Levasil suspension, stabilized at acidic pH (≈3) with a surface charge of -24 mV, it can be observed that when moving to basic pH this charge tends to become more negative, increasing the particle surface charge (in absolute value) in a progressive way. However, in the case of Ludox suspension, stabilized at basic pH (≈9) with a surface charge of -41 mV, the increment in surface charge is more marked when moving to basic pH from acidic pH. In addition, for acid pH, particles are positively charged. Therefore, there is an isoelectric point (a pH value at which there is no charge on particles surface) at pH between 3 and 4.

Figure 2 displays the flow curves for the five different feedstocks. From figure 2a (corresponding to the GS feedstock), it can be observed that this feedstock possessed a Newtonian behaviour, which is characteristic of sol–gel solutions and diluted suspensions and had a very low viscosity ($3.5 \cdot 10^{-3}$ Pa·s), which makes it suitable to be transported and injected into the plasma plume [36,44]. Moreover, thixotropy is not appreciated in figure 2a, that is a mismatch between the uploading and downloading resulting curves

which is associated to changes in the material structure or a spatial rearrangement of particles in the direction of the applied flow, since the material is totally liquid without solid particles.

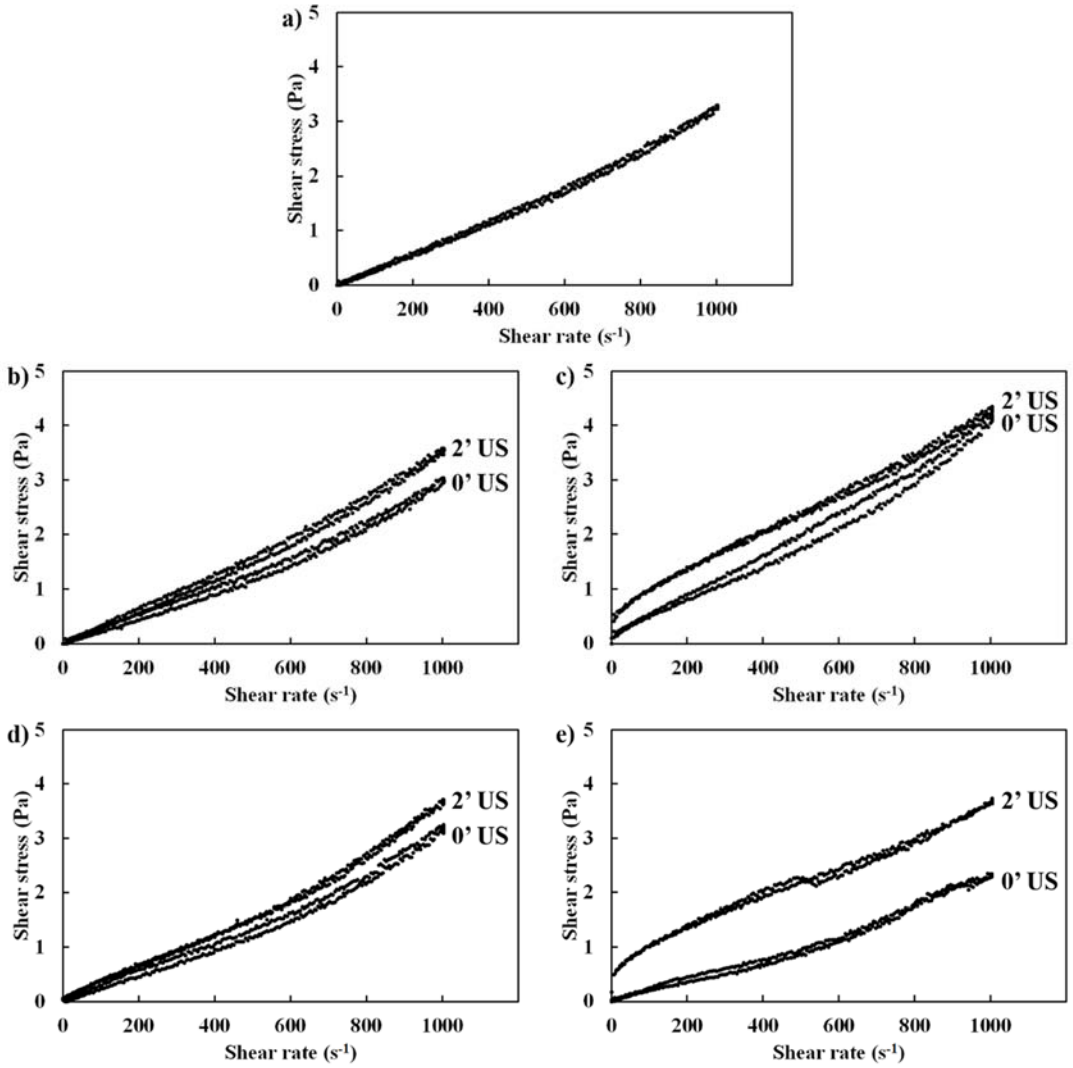

Figure 2. Flow curves of the developed feedstocks. a) GS feedstock, b) flow curves of LE05 before and after ultra–sonication, c) flow curves of LE1 before and after ultra–sonication, d) flow curves of LU05 before and after ultra–sonication and e) flow curves of LU1 before and after ultra–sonication

Concerning the substitution with Levasil CT17 suspension, the flow curves of the as–prepared LE05 and LE1 without ultra–sonication (0' US) are shown in figures 2b and 2c

respectively. In both cases the Newtonian behaviour was preserved, and there is no thixotropy despite the introduction of solid particles in the feedstock. The differences between curves from the uploading and downloading steps are due to the error of the measurement device. Viscosity values for both feedstocks are $3 \cdot 10^{-3}$ Pa·s for LE05 and $4 \cdot 10^{-3}$ Pa·s for LE1, which are very similar to that of the bioactive glass solution. Regarding the rheological behaviour, it is possible to appreciate a slight increment of the shear stress at higher shear rates, which is due to a slippage effect caused by the low viscosity of the sample close to the edge of the measuring range.

However, as the colloidal silica contained in Levasil CT17 were dispersed at pH of ≈3 and the resulting feedstocks (LE05 and LE1) had a pH lower than 2, there was a reduction of the surface charge of these colloidal particles. From figure 1a, for a pH between 1 and 2 surface charges vary from -10 mV to -15 mV approximately. There is not enough charge to avoid particles interaction, and therefore, the colloidal silica particles were destabilised when added to the mixture due to the reduction of pH, resulting in the formation and settling of agglomerates of particles.

This fact was also observed in the sedimentation tests results, which are displayed in table 5 as a maximum percentage of transmitted light after one hour of test along the cell as a function of the testing cell height. Since the analysed sample occupied a cell height from 5 to 65 mm approximately, three intervals or cell zones have been defined as shown in table 5.

Table 5. Maximum percentage of transmitted light along the vessel in function of the test vessel height for the feedstocks before and after ultra–sonication

Cell test	LE05		LE1		LU05		LU1	
	0' US	2' US	0' US	2' US	0' US	2' US	0' US	2' US
Bottom (5–25 mm)	0%	0%	0%	0%	0%	0%	0%	0%
Middle (25–45 mm)	1%	1%	1%	0%	65%	0%	85%	1%
Top (45–65 mm)	30%	1%	62%	2%	80%	1%	90%	13%

From this table, after one hour of test it can be observed in the case of LE05 that at the top of the test cell there is a 30% of transmitted light, which demonstrated that a significant sedimentation of the initially suspended colloidal particles took place and clearer sedimentation front is detected. Indeed, the higher the amount of colloidal particles added, the higher the destabilisation and, consequently, the higher the settling, as shown in table 5 for LE1 feedstock. From this table it can be observed that the maximum percentage of transmitted light at the top zone of the test cell is 62% for the LE1 feedstock. Of course, in the other zones of both feedstocks there was no transmitted light since all the settled solid concentrated in these zones.

To overcome this inconvenience, both feedstocks were subjected to ultra–sonication (UP400S, Hielscher Ultrasonics, Germany) in order to break down the agglomerates generated due to the destabilisation of the colloidal particles [45,46]. After two minutes of ultra–sonication, it is possible to confirm that without a significant increase of the feedstocks viscosity ($3.5 \cdot 10^{-3}$ Pa·s for LE05 and $4.2 \cdot 10^{-3}$ Pa·s for LE1) as shown in

figures 2b and 2c (curves labelled with 2'US), the agglomerates were broken, and the primary colloidal particles were re–dispersed again. This little differences in viscosity with regard to the feedstocks before ultra–sonication is due to the presence of well–dispersed particles which are opposing greater flow resistance. Regarding the settling, sedimentation tests were done again to both feedstocks after two minutes of ultra–sonication and results are shown in table 5. Comparing these measurements with the previous ones, it can be affirmed that the destabilisation of the colloidal particles was successfully overcome for both feedstocks (LE05 and LE1) since for the tested period (60 minutes) there was no sedimentation observed as transmittance remains at 1% and 2 % at the top cell for LE05 and LE1 feedstocks respectively.

Concerning the employment of Ludox TM–40, the flow curves of the as–prepared LU05 and LU1 are shown in figures 2d and 2e respectively (0' US). In both cases the Newtonian behaviour was preserved, and slight increment of the shear stress at higher shear rates can be also appreciated as in the Levasil CT17 utilisation. There was no significant difference in viscosity between the GS, LE05, LE1 and the LU05 ($3 \cdot 10^{-3}$ Pa·s). Contrary to that, the viscosity for LU1 was lower ($2 \cdot 10^{-3}$ Pa·s) than for the other feedstocks developed. Again, this is due to the destabilisation of the colloidal particles which, in the case of Ludox TM–40, is much more marked than in the case of the Levasil. In figure 1b, it was shown that silica particles in Ludox TM–40 were stabilised at pH ≈9, and the surface charge of the particles was dramatically reduced when the pH was moved from basic to acid values. Unlike the Levasil silica suspension, when the total substitution was carried out with Ludox silica suspension, there was a significant change of pH for the particles (from 9 to 1 approximately) during which the surface charge of the particles is significantly reduced, even going through the isoelectric point (Figure 1b) where there is no charge on the

surface of the particles. Therefore, the formation of an agglomerated structure took place, which immediately settled. Because of this, during the rheological measurements, almost all the particles settled at the bottom and the sample moved by the rotor had a much lower solids content so that there was hardly any solid material that opposed resistance to the flow. Therefore, the measurement provided an apparent lower viscosity due to the very fast sedimentation of particles.

This circumstance can be easily observed when the sedimentation test was done. Results of these tests are also shown in table 5. In both cases, the destabilisation can be clearly observed, being much more marked (as mentioned above) when the substitution was complete, since after 60 minutes of test, there was a maximum percentage of light transmittance of almost 90% along the top and the middle zones of the cell test. In fact, by this time, it was already possible to distinguish two clearly differentiated zones in the feedstock.

Due to the success in overcoming that drawback in LE05 and LE1, the other feedstocks (LU05 and LU1) were homogenised by ultra–sonication for 2 minutes, and as in the previous case (Levasil CT17), promising results were obtained. Both feedstocks were stabilised, and the colloidal particles were re–dispersed again. The viscosity of LU05 and LU1 did not pointedly increased ($3.9 \cdot 10^{-3}$ Pa·s and $4.1 \cdot 10^{-3}$ Pa·s respectively). Finally, sedimentation tests were done again to both feedstocks after two minutes of ultra–sonication and the results are included in table 5. As shown in this table, for the testing period (60 minutes) the feedstocks remained stable without particle settling. Only after one hour, a transmittance of 13% can be observed in the top zone of the cell test for the LU1. However, when comparing these results with those obtained before ultra–

sonication, after the great destabilisation of the material the outcome obtained after ultra–sounds can be considered as a promising result.

Finally, a further study of feedstocks stability over time was carried out. Each feedstock was rheologically tested at different times from its preparation and the viscosity value was taken the resulting curves. The obtained results are displayed in figure 3. As in the previously mentioned work [33], the bioactive glass solution feedstock (Figure 3a) has a stable viscosity value for 7 days, with no signs of gelation during this time. However, after the seventh day this feedstock started to gel, a process that drastically took place as reflected by the strong increase in the viscosity value of this solution between 7 and 9 days. Concerning the feedstocks with mixture of TEOS and colloidal silica suspensions, presented a similar behaviour than that of the original solution. It was expected that the lower the amount of TEOS (responsible of feedstock gelation) the higher the stability with time, but as it can be seen in figures 3b and 3c (LE05 and LU05 respectively) the gelation process took place earlier. After five days, both feedstocks started to gel in a progressive way. Despite the enhancement of colloids destabilization shown by ultra–sonication, this step had a negative effect on the feedstocks containing TEOS. When the ultra–sonication has been carried out, although the feedstocks were cooled in ice–water bath, a considerable increase in the temperature of the feedstock took place and consequently, the gelation process was accelerated due to the presence of TEOS in the solution. Regarding the LE1 and LU1 feedstocks, since TEOS was completely replaced by colloidal silica particles in both feedstocks, regardless of the ultra–sonication, there was no precursor that could cause the gelation of the feedstock. In figures 3d and 3e (LE1 and LU1 respectively) it can be seen that after 35 days from the preparation of both feedstocks they remained completely liquid and the viscosity kept constant.

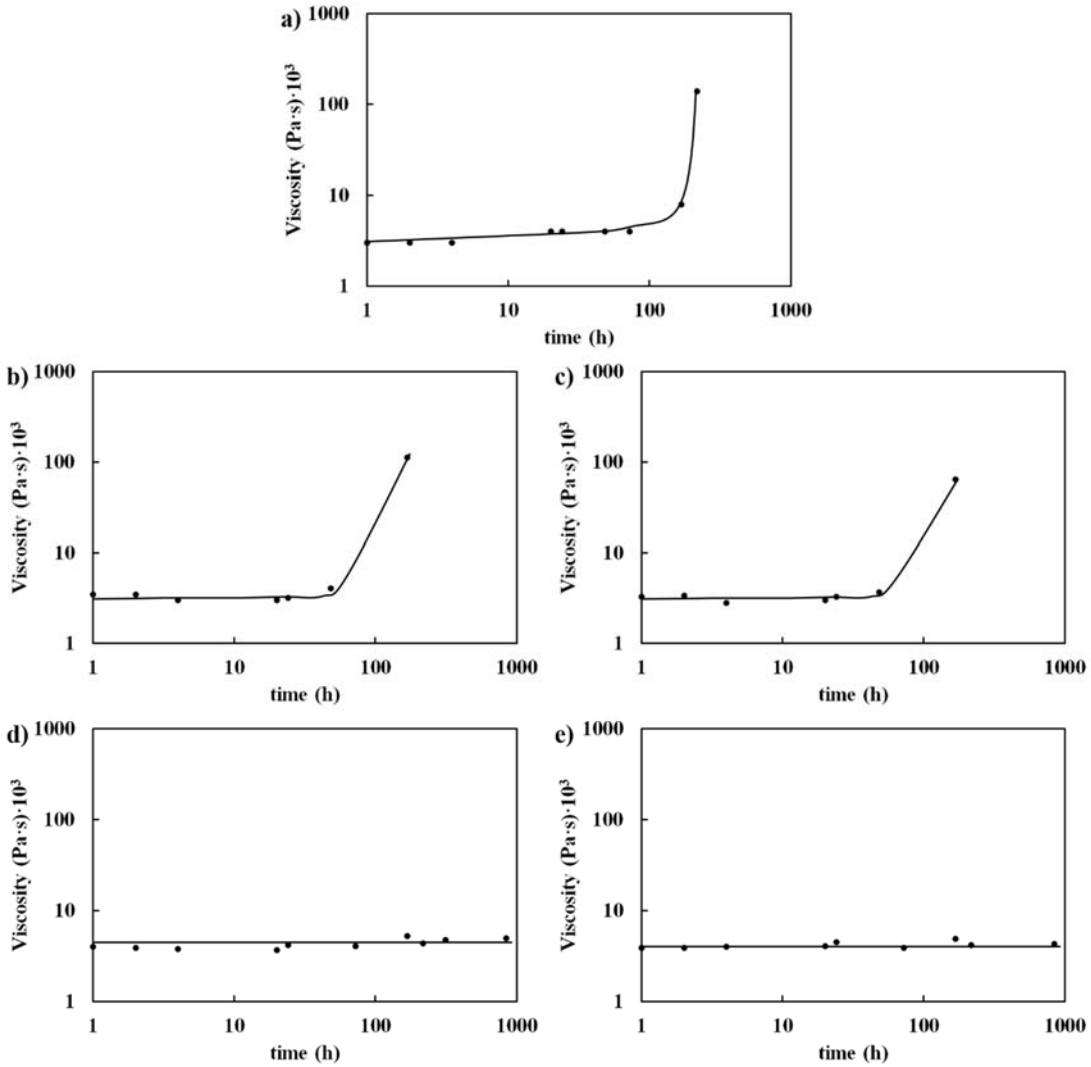

Figure 3. Stability of feedstocks with time after ultra–sonication. a) GS, b) LE05, c) LU05, d) LE1 and e) LU1

3.2. Microstructural characterisation of the coatings

The studied feedstocks were deposited by plasma spraying, as described above. Since different spraying distances were chosen and there were 5 different feedstocks, only the compositions with only precursor or colloidal silica (GS, LE1 and LU1) were sprayed in order to discriminate the effect of each silica source on the microstructure. The resulting micrographs are shown in figures 4 (surface micrographs) and 5 (cross–section micrographs) at different magnifications.

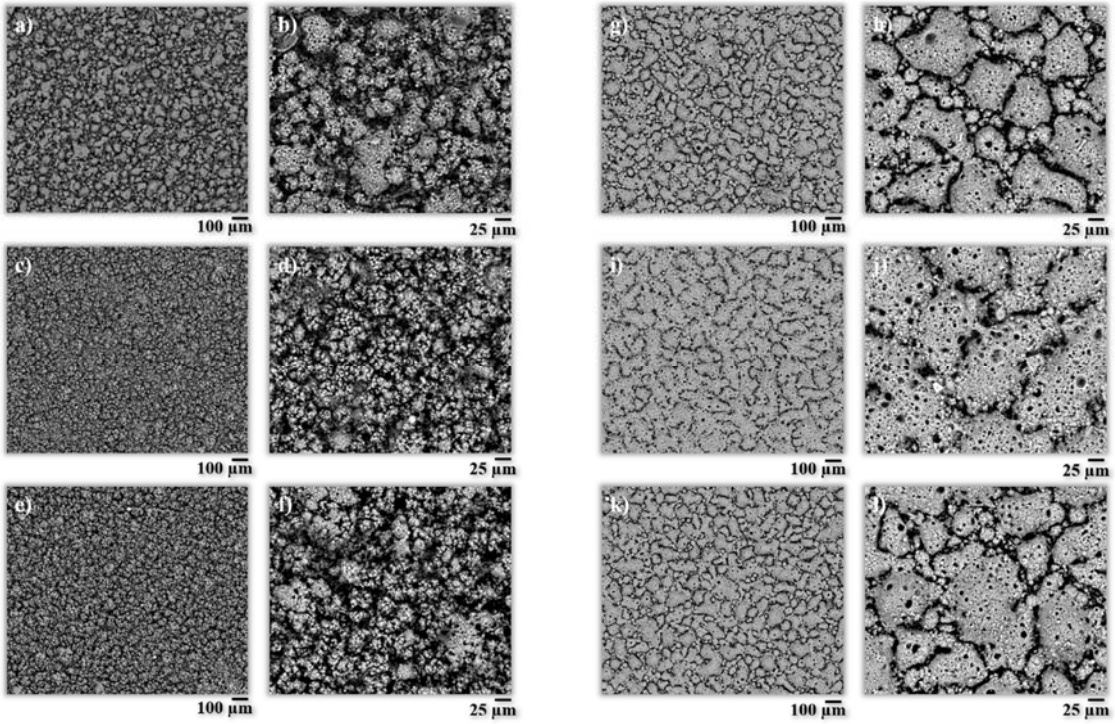

Figure 4. Surface micrographs of the deposited coatings. At 70 mm spraying distance: a) and b) GS coating (from [33]), c) and d) LE1 coating, e) and f) LU1 coating. At 40 mm spraying distance: g) and h) GS coating, i) and j) LE1 coating, k) and l) LU1 coating

From the surface examination of the obtained coatings, it can be observed that each one is completely uniform or superficially homogeneous, composed of agglomerates and deep valleys, as already found in literature about coatings deposition from liquid precursors [33,47–49]. However, a clear effect of both the spraying distance used and the presence of TEOS or colloidal silica particles can be seen in the final microstructure. The coating deposited from the original solution at 70 mm of spraying distance (figures 4a and 4b) [33], presented the two–zones microstructure typical of liquid feedstock deposition as explained, i.e. a first layer of fine glass rounded drops followed by a top layer of glass agglomerates [33,47–49], due to the high precursor concentration in the feedstock [49]. In fact, it is possible to appreciate some rounded and molten glass agglomerates on the top surface, which keep cohesive among them. Contrarily, the coatings deposited from

LE1 (figures 4c and 4d) and LU1(figures 4e and 4f) showed a surface mainly covered by small rounded glass particles that were not splatted with scarce adhesion to the substrate. There is also the presence of molten glass agglomerates, but in comparison with the coating obtained from the GS, the number of these agglomerates is very low, and they appear dispersed and isolated.

Since the spraying parameters (gases flow rates, spraying distance, arc intensity, etc.) used in the deposition of these three coatings were the same, the difference in microstructure of the coatings from silica particles with respect to the coating deposited from the bioactive glass solution can be attributed to velocity of glass formation and the difference in particle size of the glass formed inside the plasma plume. In the case of the bioactive glass solution, the hydrolysis and condensation of the TEOS was necessary in order to obtain the SiO_2 (the glass network former) by the use of a catalyst agent, therefore glass formation will take some time. In addition, in the present study nitric acid was chosen as catalyst [33]. As reported in the literature, the concentration of this catalyst affects the final particle size obtained, so that the higher the catalyst concentration, the smaller the particle size [50,51]. In fact, *Chen et al.* observed that for 1M concentration of nitric acid, the resulting distribution of bioactive glass particle sizes ranged from 1 to 5 μm, and by reducing this concentration the size distribution became wider and reached higher sizes [50]. Therefore, when using a concentration of 0.2M of nitric acid, the formation of micron–sized bioactive glass particles is expected, contrary to the case of the feedstock where SiO_2 is already in the form of particle. In these feedstocks, it is expected that the formation of glass inside the plasma plume take place earlier than for the bioactive glass solution, since the silicon dioxide is already formed as a particle. In

addition, the size of the glass drops developed will be finer since silica particles possessed colloidal size.

Hence, when GS was sprayed at 70 mm spraying distance, the formation of bioactive glass particles took place, with a particle size enough to melt before impacting onto the substrate. However, when LE1 and LU1 were sprayed at 70 mm spraying distance, as the particle size is lower than those from GS, a re–solidification of the molten drops occurred before their impact onto the substrate, resulting in a microstructure similar to that reported in [22], where "powdery" deposits were found in the coatings.

When the spraying distance was reduced from 70 to 40 mm, a significant improvement of coatings microstructure was reached. In addition, the difference in particle sizes described above also influenced the microstructure obtained by using this shorter spraying distance. Surface micrographs for coatings deposited from GS are shown in figures 4g and 4h, from LE1 in figures 4i and 4j, and for LU1 in figures 4k and 4l. For the shorter spraying distance, the three coatings exhibited a surface covered again by molten glass agglomerates onto a first layer of fine glass particles partially splashed and sintered between them. However, in all cases these agglomerates are larger than those observed for coatings obtained with 70 mm spraying distance. Due to the shorter spraying distance, the glass particles not only receive energy from the plasma plume during its flight, but also once deposited after each gun passage. As described in a previous work about suspension plasma sprayed bioactive glass coatings [16], the as–deposited glass layers are heated and softened allowing more material to adhere leading to these surface agglomerates. On the other hand, coatings obtained from LE1 and LU1 feedstocks, presented surface agglomerates more splashed and connected among them resulting in denser coatings. In opposition, it can be observed that in the case of the coating obtained

from the GS feedstock, the agglomerates are more rounded (without getting splashed at all) and separated between them. Again, this is an effect derived from the difference in size of the glass particles formed inside the plasma plume and the present colloidal ones from the novel solutions.

Regarding cross–section characterisation, apart from the coating deposited in the previous work (from GS at 70 mm spraying distance), it was only possible to examine the coatings deposited at 40 mm spraying distance from the three feedstocks. As seen above, the poor adhesion of the coatings deposited from LE1 and LU1 at 70 mm spraying distance due to their characteristic "powdery" microstructure gave rise to their total elimination during the cutting and metallographic preparation steps. The resulting cross–section micrographs of the analysed coatings are shown in figure 5 at different magnifications. When the original solution was sprayed at 70 mm distance, a homogeneous coating was obtained with a thickness of approximately 35 μm composed of small re–solidified spherical glass drops inside a molten glass matrix as described in [33]. Nevertheless, by reducing the spraying distance the obtained coatings were thicker (approximately 65 μm) than the original one, and their microstructure was substantially enhanced as explained above (surface micrographs explanation). From figures 5d, 5e and 5f, it is possible to appreciate that coating from GS feedstock deposited at 40 mm spraying distance is composed of a first layer of fine glass drops followed by a top layer of large and rounded glass agglomerates which are separated between them. Concerning the coatings deposited from the feedstocks LE1 and LU1 (figures 5g to 5l), these displayed a denser and more compact microstructure than that of the coating from the GS feedstock, with higher top glass agglomerates, which appeared more splashed and connected between them, making the coatings more regular and homogeneous. In the three cases, an open interconnected

porosity was maintained from the coating deposited from the GS feedstock at 70 mm spraying distance, which can be beneficial for the interaction with biological fluids in the potential application of the bioactive coatings.

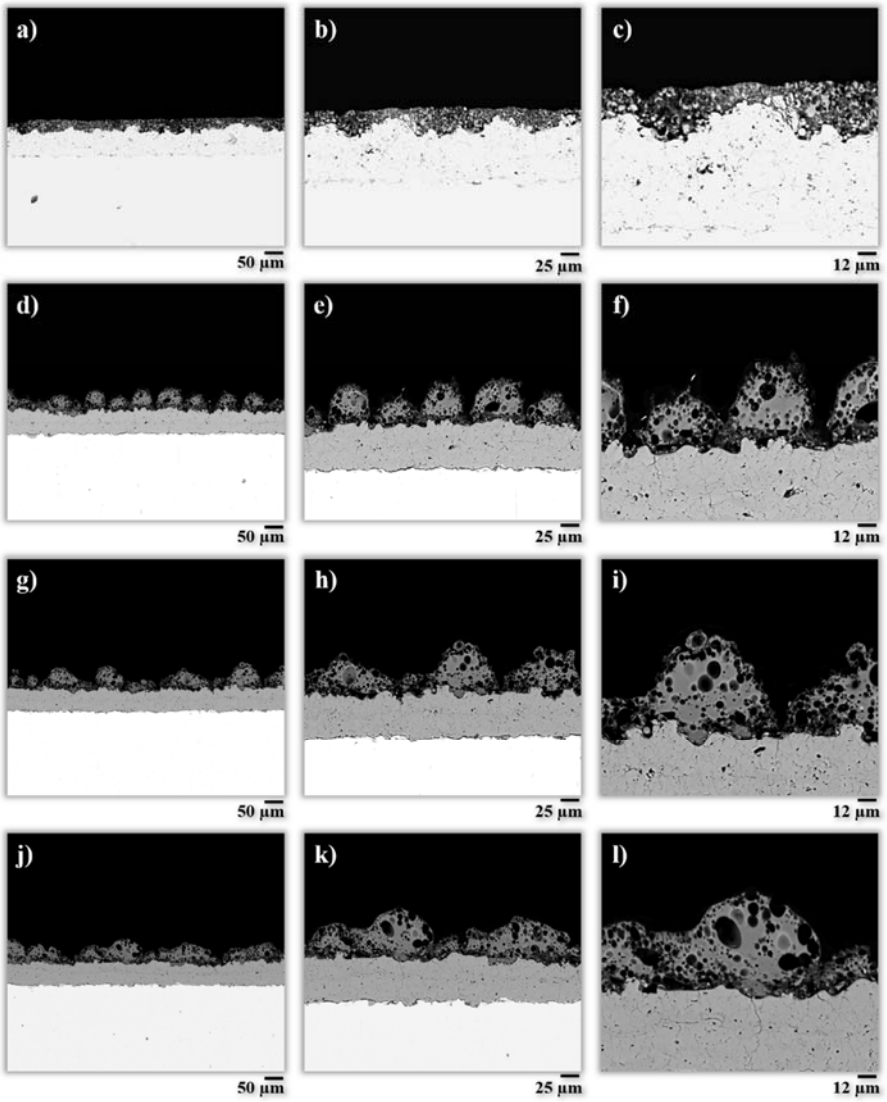

Figure 5. Cross–section micrographs of the deposited coatings. At 70 mm spraying distance: a), b) and c) GS coating (from [33]). At 40 mm spraying distance: d), e) and f) GS coating, g), h) and i) LE1 coating, j), k) and l) LU1 coating

Concerning the distribution of the bioactive glass composition elements in the coating, X-ray mapping results for the four coatings shown in figure 5, are displayed in figure 6.

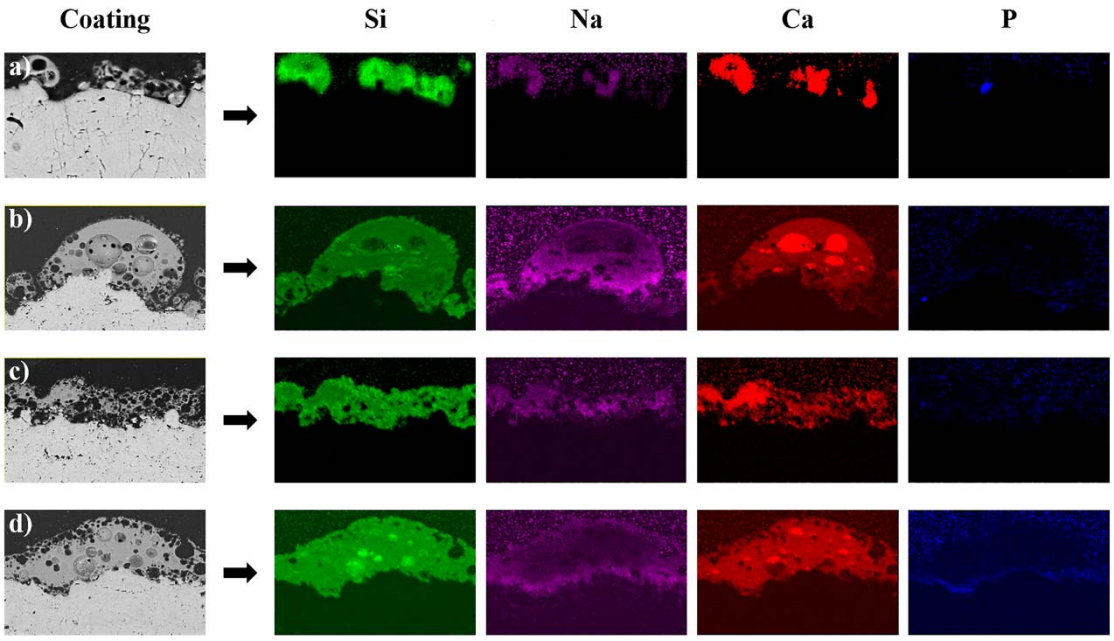

Figure 6. X–ray mapping of the deposited coatings. At 70 mm spraying distance: a) GS coating. At 40 mm spraying distance: b) GS coating, c) LE1 coating, d) LU1 coating

Regardless of the silica source and the spraying distance used, the four elements which compose the 45S5 glass are present in all coatings. As it can be seen, the distribution of the four elements is quite homogeneous in all coatings, whereas low intensity signal for phosphorous was also observed. This lack of signal could be due to the relatively low content along with a partial volatilisation of this element during the deposition process, resulting in phosphorous gas trapped in the coating contributing to form the completely rounded inner pores [52]. However, this possible deficiency of phosphorous in the coating does not avoid the development of an hydroxycarbonate apatite layer (HCA), as demonstrated in the previous work [33]. Nevertheless, it could negatively affect the rate of HCA nucleation and growth [52], which should be confirmed with further experimentation.

Finally, the XRD patterns of the six deposited coatings are displayed in figure 7. For a spraying distance of 70 mm, indistinctly of the feedstock used, the patterns shown crystalline peaks of different compounds as in the previous work.

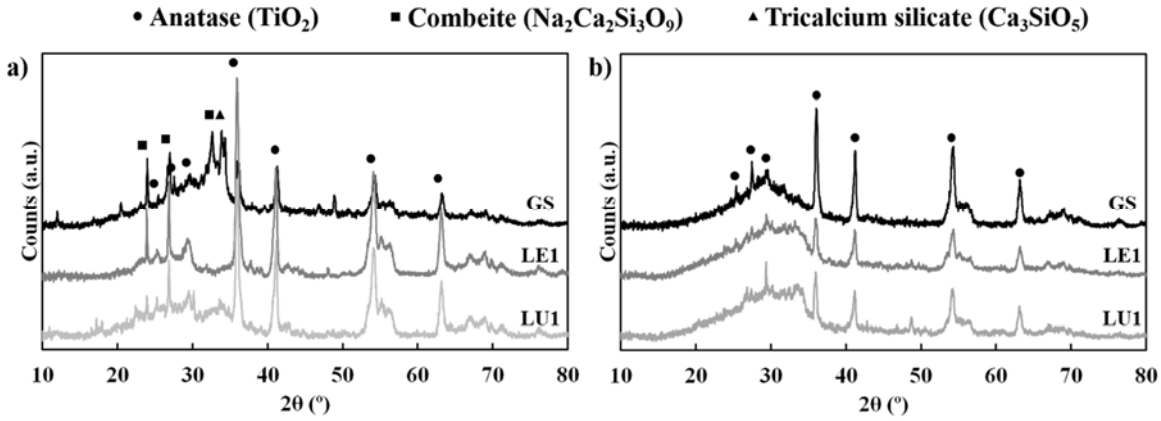

Figure 7. XRD patterns of the sprayed coatings. a) At 70 mm spraying distance for GS (from [33]), LE1 and LU1 coatings. b) At 40 mm spraying distance for GS, LE1 and LU1 coatings

Since coatings were very thin, the beam of electrons from the XRD were able to reach the bond coat and hence peaks of anatase appeared in the XRD pattern. The intensity of these peaks was higher for the coatings deposited from feedstocks containing the colloidal silica particles, since the re-solidification of the glass drops impaired their adhesion to the substrate, resulting in thinner coatings than that deposited from the GS feedstock. The other peaks correspond to the crystalline phases of combeite ($Na_2Ca_2Si_3O_9$) and tricalcium silicate (Ca_3SiO_5), which formation is due to the re-solidification of the glass drops inside the plasma plume because of the long spraying distance [33]. In fact, as described above, the re-solidification process is higher for the LE1 and LU1 feedstocks, resulting again in higher intensity crystalline peaks of combeite. For these three coatings (GS, LE1 and LU1), the developed crystallinity could be harmful for their bioactivity,

since the onset time of HCA formation because of the reaction between the glass coating and the biological media increases with the crystallinity [53,54].

Reducing the spraying distance from 70 to 40 mm prevented the glass drops inside the plasma plume from crystallization and thus, phase nature of all coatings was changed from almost crystalline to amorphous. Therefore, despite the partial vaporisation of P, the onset time of HCA formation will be shorter compared to coatings deposited under 70 mm spraying distance. Moreover, as in the previous spraying distance, the thickness of the coatings is not enough to prevent the electron beam from reaching the bond coat layer, since there was the presence of crystalline peaks of anatase in all coatings. However, compared to the previous spraying distance, coatings deposited from liquid feedstocks with colloidal silica particles at 40 mm spraying distance show less intense anatase peaks since they are denser and homogeneous, as explained above, than that deposited from the GS feedstock, whose agglomerates are more rounded and isolated.

4. Conclusions

Different liquid feedstocks were developed for the deposition of plasma sprayed 45S5 bioactive glass coatings employing TEOS, colloidal silica suspensions and mixtures of both as a source of silicon dioxide.

Colloidal silica suspensions can be a suitable material to replace TEOS in the development of 45S5 bioactive glass solutions for plasma spraying, since the resulting feedstocks possessed adequate properties to be transported and injected into the plasma plume.

Compared to the original solution, the fast formation of glass particles inside the plasma plume related to the utilisation of this colloidal silica containing feedstocks, allows only the formation of well–adhered coatings at very short spraying distances.

The microstructure of the coatings at short spraying distance results better for the feedstocks containing colloidal silica particles since it is more homogeneous and more splashed, compared to the microstructure of the coating deposited from the original solution, which is mostly composed of big glass agglomerates. However, in all cases, there was no effect of the type of feedstock in the phase nature of the coatings and the distribution of the elements of the glass composition, which were homogeneously distributed in the coatings.

More research should be done in order to assess both the mechanical properties and the bioactivity of the developed coatings and analyse the effect of the lower amount of phosphorous on these properties. In addition, new research related with the mixtures of both sources is in progress with the aim of adjusting the feedstock pH before the addition of the colloidal particles to avoid the particles destabilisation and the ultra–sonication step since it caused the premature gelation of the feedstock.

Acknowledgements

This work was supported by Universitat Jaume I (PREDOC/2015/50) and the Spanish Ministry of Economy, Industry and Competitiveness and European Regional Development Fund (MAT2015-67586-C3-R). Authors thank Dr. Encarna Blasco (ITC, Castellón, Spain) for her kindly contribution in the EDS mapping analysis step.

References

[1] J.R. Jones, A.G. Clare, Bio-glasses: An introduction (first ed.), John Wiley & Sons, Great Britain (2012).

[2] L.L. Hench, The story of Bioglass®, J. Mater. Sci. Mater. Med. 17 (2006) 967–978.

[3] M.N. Rahaman, D.E. Day, B.S. Bal, Q. Fu, S.B. Jung, L.F. Bonewald, A.P. Tomsia, Bioactive glass in tissue engineering, Acta Biomater. 7 (2011) 2355–2373.

[4] R. Li, A.E. Clark, L.L. Hench, An investigation of bioactive glass powders by sol–gel processing, J. Appl. Biomater. 2 (1991) 231–239.

[5] J. Zhong, D.C. Greenspan, Processing and properties of sol–gel bioactive glasses, J. Biomed. Mater. Res. 53 (2000) 694–701.

[6] J. Ning, A. Yao, D. Wang, W. Huang, H. Fu. X. Liu, X. Jiang, X. Zhang, Synthesis and in vitro bioactivity of a borate-based bioglass, Mater. Lett. 61 (2007) 5223–5226.

[7] A. Balamurugan, G. Balossier, S. Kannan, J. Michel, A.H.S. Rebelo, J.M.F. Ferreira, Development and in vitro characterization of sol–gel derived CaO–P2O5–SiO2–ZnO bioglass, Acta Biomater. 3 (2007) 255–262.

[8] V. Cannillo, A. Sola, Potassium-based composition for a bioactive glass, Ceram. Int. 35 (2009) 3389–3393.

[9] A. Moghanian, A. Sedghi, A. Ghorbanoghli, E. Salari, The effect of magnesium content on in vitro bioactivity, biological behavior and antibacterial activity of sol–gel derived 58S bioactive glass, Ceram. Int. 44 (2018) 9422–9432.

[10] J. Henao, C. Poblano–Salas, M. Monsalve, J. Corona–Castuera, O. Barceinas–Sánchez, Bio–active glass coatings manufactured by thermal spray: A status report, J. Mater. Res. Technol. 8 (2019) 4965–4984.

[11] Y. Liu, H. Li, B.T. Zhang, Chapter 9–Nanostructured ceramic coating biomaterials, in: G.J. Yang, X. Suo (Eds.), Advanced nanomaterials and coatings by thermal spray: Multi–dimensional design of micro–nano thermal spray coatings, Elsevier Inc., Oxford, 2019, pp. 291–311.

[12] J.P. Nayak, S. Kumar, J. Bera, Sol–gel synthesis of bioglass–ceramics using rice husk ash as a source for silica and its characterization, J. Non–cryst. Sol. 356 (2010) 1447–1451.

[13] R. Ravarian, F. Moztarzadeh, M.S. Hashjin, S.M. Rabiee, P. Khoshakhlagh, M. Tahriri, Synthesis, characterization and bioactivity investigation of bioglass/hydroxyapatite composite, Ceram. Int. 36 (2010) 291–297.

[14] A. Cattini, D. Bellucci, A. Sola, L. Pawlowski, V. Cannillo, Suspension plasma spraying of optimised functionally graded coatings of bioactive glass/hydroxyapatite, Surf. Coat. Technol. 236 (2013) 118–126.

[15] D. Stojanovic, B. Jokic, Dj. Veljovic, R. Petrovic, P.S. Uskokovic. Dj. Janackovic, Bioactive glass–apatite composite coating for titanium implant synthesized by electrophoretic deposition, J. Eur. Ceram. Soc. 27 (2007) 1595–1599.

[16] E. Cañas, M. Vicent, M.J. Orts, E. Sánchez, Bioactive glass coatings by suspension plasma spraying from glycolether-based solvent feedstock, Surf. Coat. Technol. 318 (2017) 190–197.

[17] S. Romeis, A. Hoppe, R. Detsch, A.R. Boccaccini, J. Schmidt, W. Peukert, Top–down processing of submicron 45S5 Bioglass® for enhanced in vitro bioactivity and biocompatibility, Proced. Eng. 102 (2015) 534–541.

[18] P. Fauchais, M. Vardelle, S. Goutier, A. Vardelle, Key challenges and opportunities in suspension and solution plasma spraying, Plasma Chem. Plasma Process. 35 (2015) 511–525.

[19] P. Fauchais, A. Vardelle, Innovative and emerging processes in plasma spraying: From micro– to nano–structured coatings, J. Phys. D Appl. Phys. 44 (2011) 194011.

[20] E.H. Jordan, C. Jiang, M. Gell, The solution precursor plasma spray (SPPS) process: A review with energy considerations, J. Therm. Spray Technol. 24 (2015) 1153–1165.

[21] A. Killinger, R. Gadow, G. Mauher, A. Guignard, R. Va, D. Stöver, Review of New Developments in suspension and solution precursor thermal spray processes, J. Therm. Spray Technol. 20 (2011) 677–695.

[22] L. Xie, X. Ma, A. Ozturk, E.H. Jordan. N.P. Padture, B.M. Cetegen, D.T. Xiao, M. Gell. Processing parameter effects on solution precursor plasma spray process spray patterns, Surf. Coat. Technol. 183 (2004) 51–61.

[23] E.H. Jordan, L. Xie, M. Gell, N.P. Padture, B. Cetegen, A. Ozturk, X. Ma, J. Roth, T.D. Xiao, P.E. Bryant, Superior thermal barrier coatings using solution precursor plasma spray, J. Therm. Spray Technol. 13 (2004) 57–65.

[24] M. Gell, E.H. Jordan, M. Telcholz, B.M. Cetegen, N.P. Padture, L. Xie, D. Chen, X. Ma, J. Roth, Thermal barrier coatings made by the solution precursor plasma spray process, J. Therm. Spray Technol. 17 (2008) 124–135.

[25] Y. Wang, T.W. Coyle, Solution precursor plasma spray of nickel–yittia stabilized zirconia anodes for solid oxide fuel cell application, J. Therm. Spray. Technol. 16 (2007) 898–904.

[26] P. Michaux, G. Montavon, A. Grimaud, A. Denoirjean, P. Fauchais, Elaboration of Porous NiO/8YSZ layers by several SPS and SPPS routes, J. Therm. Spray Technol. 19 (2010) 317–327.

[27] R. Dom, G. Sivakumar, N.Y. Hebalkar, S.V. Joshi, P.H. Borse, Deposition of nanostructured photocatalytic zinc ferrite films using solution precursor plasma spraying, Mater. Res. Bull. 47 (2012) 562–570.

[28] Z. Yu, H. Moussa, M. Liu, R. Schneider, M. Moliere, H. Liao, Solution precursor plasma spray process as an alternative rapid one-step route for the development of hierarchical ZnO films for improved photocatalytic degradation, Ceram. Int. 44 (2018) 2085–2092.

[29] T.W. Coyle, E. Garcia, Z. Zhang, L. Gan, Plasma spray deposition of hydroxyapatite coatings from sol precursors, Mater. Sci. Forum 539–543 (2007) 1128–1133.

[30] R.T. Candidato Jr., P. Sokołowski, L. Łatka, S. Kozerski, L. Pawłowski, A. Denoirjean, Plasma spraying of hydroxyapatite coatings using powder, suspension and solution feedstocks, Weld. Tech. Rev. 87 (2015) 64–71.

[31] R.T. Candidato Jr., C. Thouzellier, L. Pawlowski, Evaluation of the in-vitro behavior of nanostructured hydroxyapatite and zinc doped hydroxyapatite coatings obtained using solution precursor plasma spraying, J. Biomed. Mater. Res. Appl. Biomater. 106 (2018) 2101–2108.

[32] Y. Xiao, L. Song, Bioactive glass-ceramic coatings synthesized by the liquid precursor plasma spraying process, J. Therm. Spray Technol. 20 (2011) 560–568.

[33] E. Cañas, M.J. Orts, A.R. Boccaccini, E. Sánchez, Microstructural and in vitro characterization of 45S5 bioactive glass coatings deposited by solution precursor plasma spraying (SPPS), Surf. Coat. Technol. 371 (2019) 151–160.

[34] L. Xie, X. Ma, E.H. Jordan, N.P. Padture, D.T. Xiao, M. Gell, Identification of coating deposition mechanisms in the solution-precursor plasma-spray process using model spray experiments, Mater. Sci. Eng. A 362 (2003) 204–212.

[35] Y. Castro, A. Durán, R. Moreno, B. Ferrari, Thick sol–gel coatings produced by electrophoretic deposition, Adv. Mater., 14 (2002), pp. 505-508.

[36] R. Moreno, E. Bannier, Feedstock suspensions and solutions, in: N. Espallargas (Ed.), Future development of thermal spray coatings, Woodhead Publishing, Cambridge, 2015, pp. 51–80.

[37] M. Vicent, E. Bannier, P. Carpio, E. Rayón, R. Benavente, M.D. Salvador, E. Sánchez, Effect of the initial particle size distribution on the properties of suspension plasma sprayed Al_2O_3–TiO_2 coatings, Surf. Coat. Technol. 268 (2015) 209–215.

[38] P. Carpio, E. Bannier, M.D. Salvador, A. Borrell, R. Moreno, E. Sánchez, Effect of particle size distribution of suspension feedstock on the microstructure and mechanical properties of suspension plasma spraying YSZ coatings, Surf. Coat. Technol. 268 (2015) 293–297.

[39] D. Bellucci, G. Bolelli, V. Cannillo, R. Gadow, A. Killinger, L. Lusvarghi, A. Sola, N. Stiegler, High velocity suspension flame sprayed (HVSFS) potassium-based bioactive glass coatings with and without TiO_2 bond coat, Surf. Coat. Technol. 206 (2012) 3857–3868.

[40] A. Sola, D. Bellucci, V. Canillo, A. Cattini, Bioactive glass coatings: a review, Surf. Eng. 27 (2011) 560–572.

[41] P. Fauchais, Understanding plasma spraying, J. Phys. D. Appl. Phys. 37 (2004) 86–108.

[42] M.F. Smith, D.T. McGuffin, J.A. Henfling, W.J. Lenling, A comparison of techniques for the metallographic preparation of thermal sprayed samples, J. Therm. Spray Technol. 2 (1993) 287–294.

[43] J.F. Li, H.L. Liao, C.X. Ding, C. Coddet, Optimizing the plasma spray process parameters of yttria stabilized zirconia coatings using a uniform design of experiments, J. Mater. Process. Technol. 160 (2005) 34–42.

[44] A. Guignard, Development of thermal spray processes with liquid feedstocks, Schriften des Forschungszentrums Jülich Reihe Energie & Umwelt / Energy & Environment, Jülich, Germany 2012, http://www.fz-juelich.de/zb/juwel.

[45] M. Vicent, E. Sánchez, A. Moreno, R. Moreno, Preparation of high solids content nano–titania suspensions to obtain spray-dried nanostructured powders for atmospheric plasma spraying, J. Eur. Ceram. Soc. 32 (2012) 185–194.

[46] M. Vicent, E. Sánchez, G. Mallol, R. Moreno, Study of colloidal behaviour and rheology of Al_2O_3–TiO_2 nanosuspensions to obtain free–flowing spray–dried granules for atmospheric plasma spraying, Ceram. Int. 39 (2013) 8103–8111.

[47] G. Bolelli, D. Bellucci, V. Cannillo, R. Gadow, A. Killinger, L. Lusvarghi, P. Müller, A. Sola, Comparison between suspension plasma sprayed and high velocity suspension flame sprayed bioactive coatings, Surf. Coat. Technol. 280 (2015) 232–249.

[48] L. Latka, S.B. Goryachev, S. Kozerski, L. Pawlowski, Sintering of fine particles in suspension plasma sprayed coatings, Mater. 3 (2010) 3845–3866.

[49] R.T. Candidato Jr., P. Sokolowski, L. Pawlowski, G. Lecomte–Nana, C. Constantinescu, A. Denoirjean, Development of hydroxyapatite coatings by solution precursor plasma spray process and their microstructural characterization, Surf. Coat. Technol. 318 (2017) 39–49.

[50] Q.Z. Chen, Y. Li, L.Y. Jin, J.M.W. Quinn, P.A. Komesaroff, A new sol–gel process for producing Na2O–containing bioactive glass ceramics, Acta Biomater. 6 (2010) 4143–4153.

[51] B. Lei, X. Chen, Y.H. Koh, Effects of acidic catalysts on the microstructure and biological property of sol–gel bioactive glass microspheres, J. Sol–Gel Sci. Technol. 58 (2011) 656–663.

[52] O. Rojas, M. Prudent, M.E. López, F. Vargas, H. Ageorges, Influence of atmospheric plasma spraying parameters on porosity formation in coatings manufactured from 45S5 bioglass powder, J. Therm. Spray. Technol. 29 (2020) 185–198.

[53] O.P. Filho, G.P. La Torre, L.L. Hench, Effect of crystallisation on apatite-layer formation of bioactive glass 45S5, J. Biomed. Mater. Res. 30 (1996) 509–514.

[54] D.C. Clupper, J.J. Mecholsky Jr, G.P. La Torre, D.C. Greenspan, Bioactivity of tape cast and sintered bioactive glass–ceramic in simulated body fluid, Biomater. 23 (2002) 2599–2606.